Dalton Transactions

PAPER

View Article Online
View Journal

Published on 04 February 2015. Downloaded by Chinese University of Hong Kong on 19/02/2015 04:51:14.

CrossMark click for updates

Cite this: DOI: 10.1039/c4dt03791j

Metal ion-assisted ring-opening of a quinazoline-based chemosensor: detection of copper(II) in aqueous media†

Wei Cao, Xiang-Jun Zheng,* De-Cai Fang* and Lin-Pei Jin

Received 11th December 2014,
Accepted 3rd February 2015

DOI: 10.1039/c4dt03791j

www.rsc.org/dalton

A quinazoline-based fluorescence chemosensor, 6-phenol-2-yl-(5,6-dihydrobenzimidazo[1,2-*c*])quinazoline (HL), for highly selective recognition of Cu(II) in aqueous media was synthesized. The detection limit was of the order of 10^{-6} M. The crystal structures of the Cu(II) and Cd(II) complexes showed that HL changed to a Schiff base when it reacts with metal salts and that the metal ions coordinate with two nitrogen atoms and one hydroxyl oxygen atom from the Schiff base. The theoretical calculations at B3LYP-SCRF/6-31G(d) confirmed that it is the Cu(II) ion that assisted the ring-opening of the quinazoline derivative, forming a Cu(II) Schiff base complex during the detection. LMCT leads to the disappearance of fluorescence. A cell imaging study indicated that HL could be used to detect the intracellular Cu^{2+} ion.

Introduction

Fluorescent chemosensors for biologically important metal ions[1] have received considerable attention due to their high selectivity and sensitivity. Cu^{2+} plays an important role in many fundamental physiological processes, but excessive Cu^{2+} will lead to severe neurodegenerative disease.[2] The U.S. Environmental Protection Agency (EPA) has set the limit of copper in drinking water as 1.3 ppm (about 20 μM).[3] Also, the average concentration of blood copper in the normal group is 100–150 μg dL^{-1} (15.7–23.6 μM). Therefore the design and synthesis of chemosensors for detection of Cu^{2+} ions in aqueous media are very important. Quinazoline derivatives play an important role in the field of pesticides and pharmaceuticals due to their extensive biological and pharmaceutical activities.[4] This suggests that quinazoline derivatives generally have a low hazard to environment and organisms. The quinazoline derivatives synthesized using different aldehydes and 2-(2-aminophenyl)benzimidazole could be used as fluorescence chemosensors for metal ions, such as Pb^{2+}, Hg^{2+}, Cr^{3+}, Zn^{2+}, Fe^{2+}, Fe^{3+}, and Al^{3+},[5] indicating that the quinazoline derivatives can act as excellent probes for detection of metal ions. To increase the aqueous solubility and the coordination ability of the quinazoline derivative, we selected salicylaldehyde with a hydroxyl group to react with 2-(2-aminophenyl)benzimidazole to prepare the target compound, 6-phenol-2-yl-(5,6-dihydrobenzimidazo[1,2-*c*])quinazoline (HL).

Also, during the recognition process, it was reported that a solvent-assisted [1,5] sigmatropic-type shift of the secondary N–H proton from the quinazoline derivative probably occurred to result in a metal Schiff-base complex.[5a–c] Generally, the breakage of the C–N bond needs an energy of 60–90 kcal mol^{-1}.[6] It is really a challenge for the solvent to break the C–N bond of the quinazoline ring only with the assistance of a solvent. The transformation mechanism from quinazoline derivatives to Schiff bases to form the metal complexes has not yet been solved. In this context, investigating the response mechanism of quinazoline derivatives as chemosensors has become particularly important. In this paper, the detection of Cu(II) by 6-phenol-2-yl-(5,6-dihydrobenzimidazo[1,2-*c*])quinazoline (HL) was investigated. The response mechanism was discussed with a combination of experiments and theoretical calculations in detail. Also HL can be used to detect the Cu^{2+} ion in living cells by bioimaging.

Results and discussion

HL was synthesized *via* solvothermal conditions and characterized by elemental analyses, IR, ^{1}H NMR, ESI-MS and single-crystal X-ray diffraction (Fig. S1, ESI†). The single-crystal X-ray diffraction revealed that it is not a coplanar molecule because

Beijing Key Laboratory of Energy Conversion and Storage Materials, College of Chemistry, Beijing Normal University, Beijing, 100875, People's Republic of China. E-mail: xjzheng@bnu.edu.cn, dcfang@bnu.edu.cn

†Electronic supplementary information (ESI) available: Optimized Cartesian coordinates, total energies, free energies and frequencies for the stationary points located; ESI-MS, ^{1}H NMR and crystal structure of HL; competition experiments of HL with Cu^{2+} in the presence of various metal ions; changes of absorption spectra of HL upon addition of Cu^{2+} ions; Job's plot and ESI-MS of HL + Cu^{2+}; fluorescence titration. CCDC 1030199–1030201. For ESI and crystallographic data in CIF or other electronic format see DOI: 10.1039/c4dt03791j

Published on 04 February 2015. Downloaded by Chinese University of Hong Kong on 19/02/2015 04:51:14.

of the existence of a sp^3 carbon.[7] All the results showed that the quinazoline derivative has been successfully prepared.

Photophysical properties of HL

From the fluorescence spectra (Fig. 1), it can be seen that HL can emit blue light with an emission peak at 437 nm. There was no remarkable change of fluorescence intensity when Li^+, Na^+, K^+, Mg^{2+}, Ca^{2+}, Al^{3+}, Cr^{3+}, Mn^{2+}, Fe^{3+}, Ni^{2+}, Zn^{2+}, Cd^{2+}, Pb^{2+} or Hg^{2+} was added, respectively (Fig. 1 and Fig. S2a†). But addition of Cu^{2+} to HL quenched the fluorescence completely. Therefore HL was used to detect Cu^{2+} in a DMSO–H_2O (1 : 9, v/v, HEPES 20 mM, pH = 7.4) solution. The competition experiments indicated that other metal ions did not interfere with the selective recognition of HL toward Cu^{2+} (Fig. S2b†). HL could act as an efficient chemosensor for the detection of Cu^{2+}. From UV-vis absorption spectra (Fig. S2c†) we can see that compared to the absorption of HL, there are no significant changes upon addition of metal ions except Cu^{2+}. HL shows two bands at *ca.* 300 nm and a broad band at 350 nm. Upon addition of Cu^{2+} to HL, the band at 350 nm disappeared, two bands at *ca.* 300 nm became one broad band, and a new band emerged at 404 nm which could be attributed to the ligand–metal charge transfer (LMCT),[8] accompanied by the color change from colorless to yellow. With increasing the amount of Cu^{2+}, an isosbestic point could be observed at 388 nm, indicating a clear conversion of HL into the Cu(II) complex (Fig. S3†).

Species formed in the solution

To identify the species formed in the response system, three methods were adopted to obtain the Cu^{2+} complex. First, a one-pot reaction of $CuCl_2$ with salicylaldehyde and 2-(2-aminophenyl) benzimidazole under solvothermal conditions gave the single crystal of **1**. Crystallographic data and selected bond distances and angles are summarized in Tables 1 and 2, respectively. The result of single-crystal X-ray diffraction shows that it is a Cu(II)–Schiff base (L^1) complex. The Cu^{2+} ion is four-coordinated with a hydroxyl oxygen atom, an imine nitrogen and a benzimidazole nitrogen atom from L^1 and one Cl^- in a square geometry (Fig. 2a). In addition, the mixed solution of $CuCl_2$ and HL gave red crystals either under solvothermal

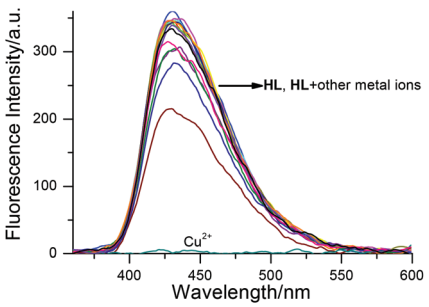

Fig. 1 Fluorescence spectra of HL (10 μM) upon the addition of 1 equiv. metal ions in DMSO–H_2O (1 : 9, v/v, HEPES 20 mM, pH = 7.4) (λ_{ex} = 352 nm).

Table 1 Crystal data and structure refinement parameters of complexes **1**, **4** and **5**[a]

Compound	**1**	**4**	**5**
Formula	$C_{20}H_{14}ClN_3OCu$	$C_{44}H_{34}N_6O_6Cd_2$	$C_{46}H_{42}N_6O_8Cd_2$
Fw	411.33	967.59	1031.68
Crystal system	Triclinic	Monoclinic	Monoclinic
Space group	$P\bar{1}$	$P2(1)/c$	$P2(1)/n$
a (Å)	8.064(6)	10.445(7)	11.633(6)
b (Å)	10.188(8)	21.759(1)	12.346(6)
c (Å)	10.856(9)	8.695(6)	14.607(7)
α (°)	90.52(1)	90	90
β (°)	105.14(1)	101.74(1)	90.26(1)
γ (°)	94.42(1)	90	90
V (Å^3)	858.2(1)	1934.9(2)	2097.9(2)
Z	2	2	2
Calculated density (Mg m^{-3})	1.592	1.661	1.633
F (000)	418	968	1040
Reflections collected/ unique	5244/3812	11 656/4449	14 307/4798
Goodness-of-fit on F^2	1.123	1.036	1.034
Final R indices [$I > 2\sigma(I)$]	R_1 = 0.0375 wR_2 = 0.0961	R_1 = 0.0304 wR_2 = 0.0721	R_1 = 0.0252 wR_2 = 0.0520
R indices (all data)	R_1 = 0.0508 wR_2 = 0.1182	R_1 = 0.0433 wR_2 = 0.0778	R_1 = 0.0352 wR_2 = 0.0558

[a] $R_1 = \sum(|F_o| - |F_c|)/|F_o|$; $wR_2 = \{\sum[(w|F_o^2| - |F_c^2|)^2/\sum w(F_o^2)^2]\}^{1/2}$.

Table 2 Selected bond distances (Å) and angles (°) for **1**, **4** and **5**

1			
Cu(1)–Cl(1)	2.237(8)	Cu(1)–N(2)	1.954(2)
Cu(1)–O(1)	1.904(2)	Cu(1)–N(3)	1.976(2)
O(1)–Cu(1)–N(2)	147.06(11)	O(1)–Cu(1)–Cl(1)	91.76(7)
O(1)–Cu(1)–N(3)	94.21(9)	N(2)–Cu(1)–Cl(1)	99.02(8)
N(2)–Cu(1)–N(3)	90.72(10)	N(3)–Cu(1)–Cl(1)	151.88(8)
4			
Cd(1)–O(3)	2.241(2)	Cd(1)–O(1)$^{\#1}$	2.278(2)
Cd(1)–O(1)	2.241(2)	Cd(1)–N(3)	2.317(2)
Cd(1)–N(2)	2.251(2)	Cd(1)–O(2)	2.535(2)
O(3)–Cd(1)–O(1)	99.74(7)	N(2)–Cd(1)–N(3)	77.07(8)
O(3)–Cd(1)–N(2)	147.59(7)	O(1)$^{\#1}$–Cd(1)–N(3)	158.61(8)
O(1)–Cd(1)–N(2)	109.70(8)	O(3)–Cd(1)–O(2)	53.80(7)
O(3)–Cd(1)–O(1)$^{\#1}$	96.24(8)	O(1)–Cd(1)–O(2)	151.45(7)
O(1)–Cd(1)–O(1)$^{\#1}$	79.11(6)	N(2)–Cd(1)–O(2)	94.42(7)
N(2)–Cd(1)–O(1)$^{\#1}$	102.25(7)	O(1)$^{\#1}$–Cd(1)–O(2)	111.25(7)
O(3)–Cd(1)–N(3)	94.91(8)	N(3)–Cd(1)–O(2)	90.05(7)
O(1)–Cd(1)–N(3)	81.05(7)		
Symmetry code: #1 $-x + 1, -y + 1, -z + 1$			
5			
Cd(1)–N(1)	2.250(2)	Cd(1)–O(1)$^{\#2}$	2.303(1)
Cd(1)–O(3)	2.280(2)	Cd(1)–N(3)	2.318(2)
Cd(1)–O(1)	2.290(1)	Cd(1)–O(2)	2.452(2)
N(1)–Cd(1)–O(3)	117.52(6)	O(1)–Cd(1)–N(3)	81.75(5)
N(1)–Cd(1)–O(1)	153.27(6)	O(1)$^{\#2}$–Cd(1)–N(3)	162.86(5)
O(3)–Cd(1)–O(1)	84.32(5)	N(1)–Cd(1)–O(2)	80.14(6)
N(1)–Cd(1)–O(1)$^{\#2}$	114.71(6)	O(3)–Cd(1)–O(2)	159.27(6)
O(3)–Cd(1)–O(1)$^{\#2}$	82.81(5)	O(1)–Cd(1)–O(2)	82.29(6)
O(1)–Cd(1)–O(1)$^{\#2}$	81.41(5)	O(1)$^{\#2}$–Cd(1)–O(2)	79.60(6)
N(1)–Cd(1)–N(3)	79.90(6)	N(3)–Cd(1)–O(2)	95.02(6)
O(3)–Cd(1)–N(3)	98.65(6)		
Symmetry code: #2 $-x + 1, -y, -z$			

This journal is © The Royal Society of Chemistry 2015

Published on 04 February 2015. Downloaded by Chinese University of Hong Kong on 19/02/2015 04:51:14.

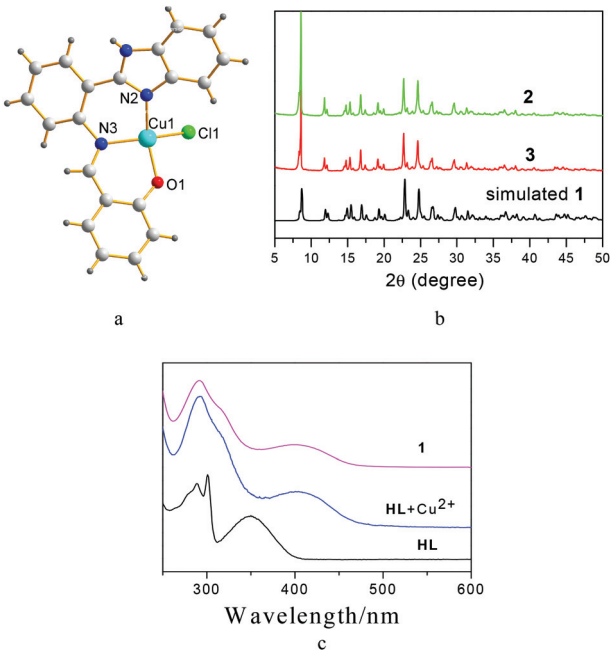

Fig. 2 (a) Crystal structure of the complex **1** with an atom labelling; (b) powder X-ray diffraction patterns of **1**, **2** and **3**; (c) the absorption spectra of complex **1**, HL+ 1 equiv. Cu^{2+} (HL + Cu^{2+}) and HL.

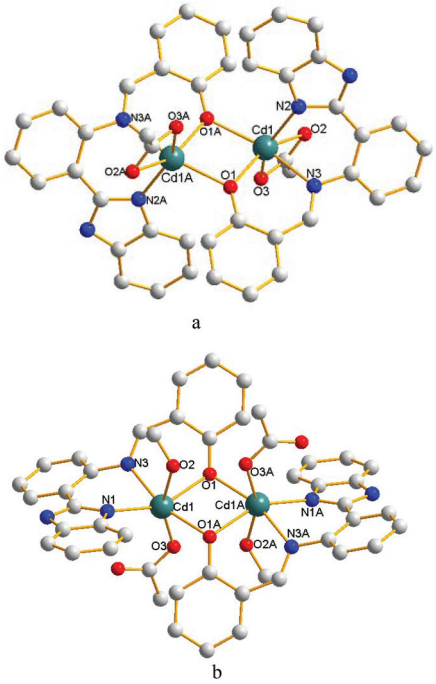

Fig. 3 (a) Crystal structure with an atom labelling for **4**, symmetry code: A: $-x + 1$, $-y + 1$, $-z + 1$; (b) crystal structure with an atom labelling for **5**, symmetry code: A: $-x + 1$, $-y$, $-z$.

conditions (**2**) or after slow evaporation at room temperature (**3**). Crystals of **2** and **3** were characterized by elemental analyses, IR, and powder X-ray diffraction (Fig. 2b). The results show that **2** and **3** are the same complex as **1**, which implies that the C–N bond in HL was broken to become a benzimidazole-based Schiff base (HL^1) with more chelating sites to bind Cu^{2+}, resulting in the formation of complex **1**.

Furthermore, it was observed that the absorption spectrum of the system HL + Cu^{2+} was different from that of HL, but the same as that of complex **1** (Fig. 2c), indicating that complex **1** was formed in the system. The Job's plot indicated that HL binds Cu(II) to form a 1 : 1 Cu–L^1 complex (Fig. S4†). To gain an insight into the stoichiometry of the Cu–L^1 complex, the electrospray ionization mass spectrum was recorded (Fig. S5†). A peak appearing at *m*/*z* 375.02 was attributed to Cu–L^1 with a 1 : 1 binding mode (calculated $[CuL^1]^+$ *m*/*z* is 374.90), while the peak at *m*/*z* 453.03 can be ascribed to $[CuL^1DMSO]^+$ (calcd. 453.03). All the above results indicated that upon the addition of Cu^{2+} to the solution of HL, HL changed to HL^1, and that the formation of **1** resulted in fluorescence quenching of HL. Based on the fluorescence titrations, the detection limit for Cu^{2+} was 7.1 μM and the association constant ($\log K_a$) deduced for 1 : 1 stoichiometry was 4.7 (Fig. S6†).[9] The detection limit was lower than the limit of copper in drinking water defined by the U.S. EPA limit (~20 μM).[3]

Considering copper has a changeable valence in complexes, we selected a d^{10} metal ion, Cd^{2+}, to investigate its corresponding complexes, the preparation of which is similar to those of complexes **1** and **2**. Orange and yellow crystals were obtained and characterized by single-crystal X-ray diffraction to be $[CdL^1(Ac)]_2$ (**4**) and $[CdL^1(Ac)(CH_3OH)]_2$ (**5**), respectively. They have binuclear molecular structures (Fig. 3a and 3b). For Cd^{2+} ions, similarly to Cu^{2+}, after one-pot reaction of the tri-component or direct reaction of Cd^{2+} ions with HL, a Schiff base complex was formed. The Schiff base L^1 adopts a tetradentate coordination mode to link two Cd^{2+} ions. Cd^{2+} ions in **4** and **5** are both six-coordinated in a distorted octahedral geometry. The structures of **1**–**5** directly support the ring-opening of the quinazoline compound HL to become the Schiff-base in the Cu(II) and Cd(II) complexes. The results indicated that ring-opening of HL is assisted by the binding of HL with metal ions.

Ring-opening and fluorescence quenching of HL by Cu^{2+}

To explore the probable reaction of HL + $CuCl_2$ → $[CuL^1Cl]$ + HCl, the B3LYP-SCRF/6-31G(d) method has been employed to characterize the energies, structures and frequencies. The probable reaction pathway and relative energy are schematically described in Fig. 4, from which one can see that the formation of COM1 would release free energy of 29.7 kcal mol^{-1}. After that one of the Cl atoms in $CuCl_2$ would take a hydrogen atom in the OH group to form an HCl molecule, and then the hydrogen atom in the HCl molecule could be easily transferred into an N atom in the imidazole ring to form INT2 without any transition state, releasing the free energy of 9.3 kcal mol^{-1}. Breaking the C–N bond is the rate-controlling step in this reaction, with the free energy barrier being 21.8 kcal mol^{-1}, which is easy to overcome under experimental conditions. As we know, the bond energy of the C–N bond in HL has been calcu-

Published on 04 February 2015. Downloaded by Chinese University of Hong Kong on 19/02/2015 04:51:14.

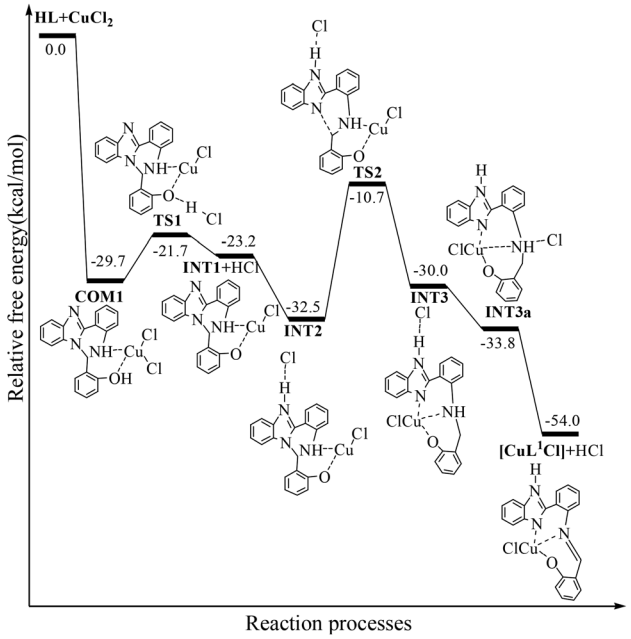

Fig. 4 The relative energy (kcal mol^{-1}) at B3LYP-SCRF/6-31G(d) for the stationary points during the reaction of HL + $CuCl_2$ → [CuL^1Cl] + HCl.

lated to be 69.3 kcal mol^{-1}, which is hard to overcome without the assistance of $CuCl_2$. In INT2, TS2 and INT3, the Cl atom bonded to a hydrogen atom holds a charge of *ca.* −0.85e, and thus it is in fact Cl^-, which is only loosely bonded to NH and probably could be freely moved in solution. Therefore, the formation of INT3a is also a favorable process, releasing a free energy of 3.8 kcal mol^{-1}, and then the release of an HCl molecule would further lower the free energy by 21.2 kcal mol^{-1}, indicating that this is an automatic process.

In order to elucidate the fluorescence quenching of HL upon the addition of Cu^{2+}, the LMCT mechanism for the complex [CuL^1Cl] was calculated. The frontier orbitals and energy levels are depicted in Fig. 5, from which one can realize that HOMO is mainly on a phenyl ring of ligand (L^1) and LUMO is an empty d orbital; therefore, the overlap of HOMO and LUMO is almost zero, *i.e.*, the excitation of HOMO to LUMO is not allowed. Although the overlap between HOMO and LUMO+1 is not very big, excitation between HOMO and LUMO+1 seems possible. Once one electron is excited to LUMO+1, the electron could be transferred into LUMO orbital (d orbital of Cu) from LUMO+1 (on L^1). Then the electron could not return to HOMO, leading to the disappearance of fluorescence.

Cell imaging studies

Owning to the encouraging selectivity and sensitivity of HL toward Cu^{2+} ions, bioimaging experiments were conducted to prove the ability of HL to detect Cu^{2+} in living cells. HeLa cells were first incubated with 20 μM HL for 2 h, and then treated with 10 μM $CuCl_2$ for 15 min. As shown in Fig. 6, intensive

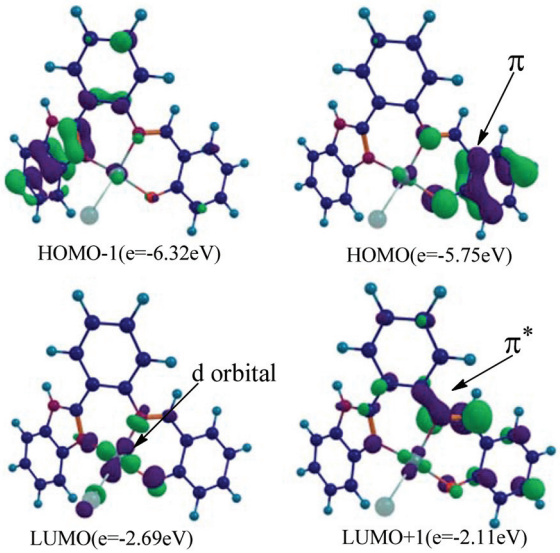

Fig. 5 The frontier orbitals and their orbital energies for [CuL^1Cl].

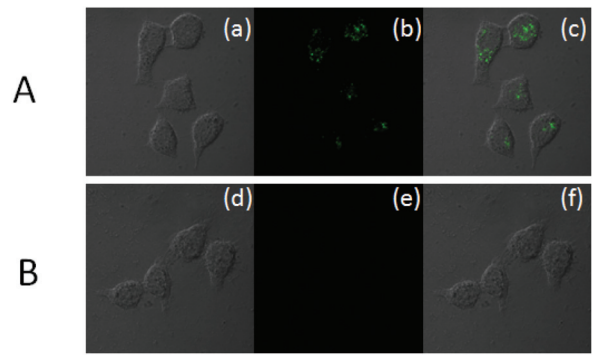

Fig. 6 Live-cell imaging of HeLa cells treated with **HL** before (A) and after (B) incubation with $CuCl_2$. (a) and (d) represent the bright-field images, (b) and (e) represent the fluorescence images, and (c) and (f) represent the overlay images (λ_{ex} = 405 nm).

fluorescence was observed when HeLa cells were exposed to HL, while the bright fluorescence can be quenched completely by further incubation of the cells with Cu^{2+}. These results demonstrated that HL is cell-permeable and can respond to copper(II) ions within living cells.

Conclusions

In summary, a quinazoline derivative, 6-phenol-2-yl-(5,6-dihydrobenzimidazo[1,2-*c*])quinazoline (HL), was synthesized and characterized. HL showed highly selective and sensitive fluorescence 'on–off' behaviour toward Cu^{2+}, and it can be used to detect the Cu^{2+} ion in living cells by bioimaging. The fluorescence quenching of HL upon the addition of Cu^{2+} ions was due to LMCT in **1**. The combination of experimental observations and theoretical calculations indicated that it is the

This journal is © The Royal Society of Chemistry 2015

Published on 04 February 2015. Downloaded by Chinese University of Hong Kong on 19/02/2015 04:51:14.

binding of HL with metal ions that leads to the ring-opening of HL.

Experimental section

General information and materials

All solvents and reagents (analytical grade) were used as received. Elemental analyses were conducted using a Vario EL elemental analyzer. Fourier transform infrared (FT-IR) spectra were recorded on an Avatar 360 FI-IR spectrometer using KBr pellets. UV-Vis absorption spectra were recorded using a spectrophotometer UV-2450, and fluorescence spectra were recorded on a Cary Eclipse fluorescence spectrophotometer, with a quartz cuvette (path length = 1 cm). ^{1}H NMR spectra were obtained using a Bruker Avance III 400 MHz spectrometer. Mass spectra (ESI) were recorded on an LCT Premier XE time-of-flight (TOF) mass spectrometer.

Synthesis of $C_{20}H_{15}N_3O$ (HL)

A methanol (3 mL) solution of salicylaldehyde (0.2 mmol, 0.020 mL) and 2-(2-aminophenyl)benzimidazole (0.2 mmol, 0.042 g) was sealed in a Teflon-lined stainless steel autoclave and heated at 80 °C for 3 days, and then cooled to room temperature. Yellow crystals suitable for X-ray crystallography were obtained (yield 71.9%). Anal. Calcd for $C_{20}H_{15}N_3O$ (%): C, 76.66; H, 4.83; N, 13.41. Found: C, 76.54; H, 4.65; N, 13.00. IR (KBr pellet, cm^{-1}): 3417s, 3051w, 2699w, 1618s, 1535s, 1499s, 1401s, 1322m, 1288s, 1242s, 1159m, 1111m, 863w, 738s.

One-pot synthesis of [CuL^{1}Cl] (1)

A methanol (5 mL) solution of $CuCl_2{\cdot}2H_2O$ (0.1 mmol, 0.017 g), 2-(2-aminophenyl)benzimidazole (0.2 mmol, 0.042 g) and salicylaldehyde (0.2 mmol, 0.020 mL) was sealed in a Teflon-lined stainless steel autoclave and heated at 80 °C for 3 days, and then cooled to room temperature. Deep red crystals suitable for X-ray crystallography were obtained (yield 78.3%). Anal. Calcd for $C_{20}H_{14}ClN_3OCu$ (%): C, 58.39; H, 3.43; N, 10.21. Found: C, 58.02; H, 3.62; N, 10.00. IR (KBr pellet, cm^{-1}): 3443w, 3184w, 3067w, 1609s, 1590w, 1531s, 1487m, 1463m, 1442s, 1385m, 1322m, 1184s, 1143m, 760s.

Synthesis of [CuL^{1}Cl] (2)

A methanol (3 mL) solution of $CuCl_2{\cdot}2H_2O$ (0.1 mmol, 0.017 g) and HL (0.1 mmol, 0.031 g) was sealed in a Teflon-lined stainless steel autoclave and heated at 80 °C for 3 days, and then cooled to room temperature. Deep red crystals were obtained in 54.9% yield. Anal. Calcd for $C_{20}H_{14}ClN_3OCu$ (%): C, 58.39; H, 3.43; N, 10.21. Found: C, 58.18; H, 3.47; N, 10.14. IR (KBr pellet, cm^{-1}): 3445w, 3184w, 3065w, 1609s, 1590w, 1531s, 1489s, 1463s, 1442s, 1386s, 1323m, 1184s, 1143m, 760s.

Synthesis of [CuL^{1}Cl] (3)

HL (0.1 mmol, 0.031 g) was dissolved in DMSO (1 mL), and then a methanol (3 mL) solution of $CuCl_2{\cdot}2H_2O$ (0.1 mmol, 0.017 g) was added into the solution of HL. Upon slow evaporation of the solvents at room temperature, deep red crystals were obtained over a period of 4 days in 29.2% yield. Anal. Calcd for $C_{20}H_{14}ClN_3OCu$ (%): C, 58.39; H, 3.43; N, 10.21. Found: C, 57.91; H, 3.54; N, 9.98. IR (KBr pellet, cm^{-1}): 3445w, 3182w, 3064w, 1609s, 1590w, 1531s, 1489s, 1463s, 1441s, 1385s, 1322m, 1184s, 1143m, 760s.

One-pot synthesis of [CdL^1(Ac)]$_2$ (4)

4 was synthesized as complex **1** except that $CuCl_2{\cdot}2H_2O$ was replaced by $Cd(Ac)_2{\cdot}2H_2O$. Orange crystals suitable for X-ray crystallography were obtained (yield 30.0%). Anal. Calcd for $C_{22}H_{17}N_3O_3Cd$ (%): C, 54.62; H, 3.54; N, 8.68. Found: C, 54.52; H, 3.47; N, 8.63. IR (KBr pellet, cm^{-1}): 3395w, 3058w, 2900w, 1605s, 1573s, 1531s, 1438m, 1301s, 1176m, 1159s, 1044m, 817m, 754s.

Synthesis of [CdL^1(Ac)(CH$_3$OH)]$_2$ (5)

5 was synthesized as complex **2** except that 0.1 mmol $CuCl_2{\cdot}2H_2O$ was replaced by 0.05 mmol $Cd(Ac)_2{\cdot}2H_2O$. Yellow crystals suitable for X-ray crystallography were obtained (yield 40.2%). Anal. Calcd for $C_{23}H_{21}N_3O_4Cd$ (%): C, 53.55; H, 4.10; N, 8.15. Found: C, 53.67; H, 4.14; N, 8.08. IR (KBr pellet, cm^{-1}): 3418w, 3071w, 2900w, 1603s, 1531s, 1436s, 1306m, 1175m, 1158s, 1044m, 818m, 759s.

X-ray crystallography

Single-crystal X-ray diffraction data of HL, **1**, **4** and **5** were collected on a Bruker APEX II CCD diffractometer with graphite monochromated Mo-Kα radiation (λ = 0.71073 Å) at 293 K. The structures were solved by direct methods and refined by full matrix least squares based on F^2 using the SHELX 97 program.[10] All non-hydrogen atoms were refined anisotropically. Hydrogen atoms were placed in calculated positions. CCDC no. 1030199–1030201 contains the supplementary crystallographic data for this paper.

Methods for cell imaging

The HeLa cell line was cultured in DMEM (Dulbecco's modified Eagle medium). Cells were incubated with 20 μM of **HL** at 37 °C for 2 h. After washing with PBS three times to remove the remaining **HL**, the cells were then incubated with 7.5 μM $CuCl_2{\cdot}2H_2O$ for 15 min at room temperature. The incubated cells were washed with PBS and mounted onto a glass slide. The fluorescent images of the mounted cells were obtained using a confocal laser scanning microscope with 405 nm excitation.

Calculation methods

In this work, quantum chemical calculations were carried out using the Gaussian 09 program package.[11] The possible ground state structures have been optimized with density functional theory (DFT) at the B3LYP/6-31G(d) level,[12] in which the effect of the solvent has been considered using the polarized continuum model (PCM)[13] with the corresponding solvent,

Published on 04 February 2015. Downloaded by Chinese University of Hong Kong on 19/02/2015 04:51:14.

such as methanol, DMF and DMSO. On the basis of the optimized configuration for the ground state, TD-DFT[14] calculations were performed using the B3LYP functional (TD-B3LYP-SCRF) within the adiabatic approximation to predict the excitation energies, which will provide information on the fluorescence properties of the studied species.

Acknowledgements

This work was supported by the National Natural Science Foundation of China (20971015) and the Fundamental Research Funds for the Central Universities.

Notes and references

1 (*a*) A. P. de Silva, H. Q. N. Gunaratne, T. Gunnlaugsson, A. J. M. Huxley, C. P. McCoy, J. T. Rademacher and T. E. Rice, *Chem. Rev.*, 1997, **97**, 1515–1566; (*b*) B. Valeur and I. Leray, *Coord. Chem. Rev.*, 2000, **205**, 3–40; (*c*) Z. P. Liu, W. J. He and Z. J. Guo, *Chem. Soc. Rev.*, 2013, **42**, 1568–1600.

2 E. Gaggelli, H. Kozlowski, D. Valensin and G. Valensin, *Chem. Rev.*, 2006, **106**, 1995–2044.

3 W. T. Tak and S. C. Yoon, *Korean J Nephrol.*, 2001, **20**, 863–871.

4 (*a*) D. Wang and F. Gao, *Chem. Cent. J.*, 2013, **7**, 95; (*b*) M. N. Noolvi, H. M. Patel, V. Bhardwaj and A. Chauhan, *Eur. J. Med. Chem.*, 2011, **46**, 2327–2346; (*c*) X. Wu, M. Li, W. Tang, Y. Zheng, J. Lian, L. Xu and M. Ji, *Chem. Biol. Drug Des.*, 2011, **78**, 932–940.

5 (*a*) U. C. Saha, B. Chattopadhyay, K. Dhara, S. K. Mandal, S. Sarkar, A. R. Khuda-Bukhsh, M. Mukherjee, M. Helliwell and P. Chattopadhyay, *Inorg. Chem.*, 2011, **50**, 1213–1219; (*b*) S. Sen, S. Sarkar, B. Chattopadhyay, A. Moirangthem, A. Basu, K. Dharad and P. Chattopadhyay, *Analyst*, 2012, **137**, 3335–3342; (*c*) M. Makherjee, B. Sen, S. Pal, M. S. Hundal, S. K. Mandal, A. R. Khuda-Bukhsh and P. Chattopadhyay, *RSC Adv.*, 2013, **3**, 19978–19984; (*d*) D. Jeyanthi, M. Iniya, K. Krishnaveni and D. Chellappa, *RSC Adv.*, 2013, **3**, 20984–20989; (*e*) L. Tang, N. Wang, Q. Zhang, J. Guo and R. Nandhakumar, *Tetrahedron Lett.*, 2013, **54**, 536–540; (*f*) P. Saluja, N. Kaur, N. Singh and D. O. Jang, *Tetrahedron*, 2012, **68**, 8551–8556; (*g*) R. Pandey, R. K. Gupta, M. Shahid, B. Maiti and A. Misra, *Inorg. Chem.*, 2012, **51**, 298–311; (*h*) B. Sen, M. Makherjee, S. Pal, S. K. Mandal, M. S. Hundal, A. R. Khuda-Bukhsh and P. Chattopadhyay, *RSC Adv.*, 2014, **4**, 15356–15362; (*i*) A. Kumar, R. Pandey, A. Kumar and D. S. Pandey, *RSC Adv.*, 2014, **4**, 55967–55970; (*j*) M. Mukherjee, B. Sen, S. Pal, S. Banerjee, S. Lohar and P. Chattopadhyay, *RSC Adv.*, 2014, **4**, 64014–64020.

6 D. E. Lide, *CRC Handbook of Chemistry and Physics*, CRC Press, Florida, Boca Raton, 82th edn, 2002.

7 N. E. Eltayeb, S. G. Teoh, C. K. Quah and H.-K. Fun, *Acta Crystallogr., Sect. E: Struct. Rep. Online*, 2011, **67**, o2243–o2244.

8 (*a*) E. I. Solomon, M. J. Baldwin and M. D. Lowery, *Chem. Rev.*, 1992, **92**, 521–542; (*b*) R. C. Holz, J. M. Brink, F. T. Gobena and C. J. O'Connor, *Inorg. Chem.*, 1994, **33**, 6086–6092; (*c*) W. Cao, X. J. Zheng and L. P. Jin, *Dalton Trans.*, 2014, **43**, 7298–7303.

9 H. A. Benesi and J. H. Hildebrand, *J. Am. Chem. Soc.*, 1949, **71**, 2703–2707.

10 G. M. Sheldrick, *SHELXS-97, Program for solution of crystal structures*, University of Göttingen, Germany, 1997.

11 M. J. Frisch, G. W. Trucks, H. B. Schlegel, G. E. Scuseria, M. A. Robb, J. R. Cheeseman, G. Scalmani, V. Barone, B. Mennucci, G. A. Petersson, H. Nakatsuji, M. Caricato, X. Li, H. P. Hratchian, A. F. Izmaylov, J. Bloino, G. Zheng, J. L. Sonnenberg, M. Hada, M. Ehara, K. Toyota, R. Fukuda, J. Hasegawa, M. Ishida, T. Nakajima, Y. Honda, O. Kitao, H. Nakai, T. Vreven, J. A. Montgomery, J. E. Peralta Jr., F. Ogliaro, M. Bearpark, J. J. Heyd, E. Brothers, K. N. Kudin, V. N. Staroverov, T. Keith, R. Kobayashi, J. Normand, K. Raghavachari, A. Rendell, J. C. Burant, S. S. Iyengar, J. Tomasi, M. Cossi, N. Rega, J. M. Millam, M. Klene, J. E. Knox, J. B. Cross, V. Bakken, C. Adamo, J. Jaramillo, R. Gomperts, R. E. Stratmann, O. Yazyev, A. J. Austin, R. Cammi, C. Pomelli, J. W. Ochterski, R. L. Martin, K. V. Morokuma, G. Zakrzewski, G. A. Voth, P. Salvador, J. J. Dannenberg, S. Dapprich, A. D. Daniels, O. Farkas, J. B. Foresman, J. V. Ortiz, J. Cioslowski and D. J. Fox, *Gaussian 09*, Gaussian, Inc., Wallingford CT, 2010.

12 A. D. Becke, *J. Chem. Phys.*, 1982, **65**, 239–245.

13 (*a*) M. Cossi, V. Barone, R. Cammi and J. Tomasi, *Chem. Phys. Lett.*, 1996, **255**, 327–335; (*b*) G. Scalmani and M. J. Frisch, *J. Chem. Phys.*, 2010, **132**, 114110–114124.

14 (*a*) F. Furche and R. Ahlrichs, *J. Chem. Phys.*, 2002, **117**, 7433–7447; (*b*) G. Scalmani, M. J. Frisch, B. Mennucci, J. Tomasi, R. Cammi and V. Barone, *J. Chem. Phys.*, 2006, **124**, 094107.

 This journal is © The Royal Society of Chemistry 2015